RSC Advances

ROYAL SOCIETY OF CHEMISTRY

www.rsc.org/advances

Cite this: DOI: 10.1039/c0xx00000x

www.rsc.org/xxxxxx

ARTICLE TYPE

Semiconductor $Pb_2P_2S_6$ and Size-Dependent Band Gap Energy of Its Nanoparticles

Xian Zhang,[a] Jianqiao He,[b] Wei Chen,[a] Chao Wang,[c] Chong Zheng,[d] Jianhua Lin,*[a] Xia Zhang*[e] and Fuqiang Huang*[a,b]

Received (in XXX, XXX) Xth XXXXXXXXX 20XX, Accepted Xth XXXXXXXXX 20XX
DOI: 10.1039/b000000x

Microcrystalline $Pb_2P_2S_6$ powder was synthesized via a traditional melting salt method with KI or LiBr/KBr mixture (mole ratio is 3/2) acting as flux. The nanostructured $Pb_2P_2S_6$ powder was further synthesized by a high-speed ball milling technique. The $Pb_2P_2S_6$ powder was investigated by scanning electron microscopy (SEM), powder X-ray diffraction (XRD), optical absorption (UV-vis) and photoluminescence measurements. The average particle size of the nanostructured $Pb_2P_2S_6$ powder changes from 500 to 60 nm when increasing the milling time from 0.5 h to 4 h. The optical properties of the $Pb_2P_2S_6$ powder show a size-dependence, with the band gap ranging from 2.56 eV to 2.88 eV. First-principle calculation reveals that the $Pb_2P_2S_6$ is a semiconductor with an indirect band gap of 2.15 eV. The size-dependence nature also makes the photoluminescence properties of the material tunable.

Introduction

Semiconductor nanoparticles (NPs) receive a great deal of interest due to their size-dependent properties.[1-4] The optical absorption and emission properties of these NPs can easily be tuned due to the quantum confinement effect.[4] In particular for the cadmium analogues, the emissions and absorptions of them can be tuned within all visible light range.[5] Among these NPs, the lead chalcogenide quantum dots (QDs) have received great attention not only because of their applications in the third-generation solar cells,[6-19] but also owing to their size-dependent optical properties.[7, 20-28] The band gaps of the bulk lead chalcogenides are small (0.37 eV for PbS and 0.27 eV for PbSe[18, 21-22, 29]), but due to the very large confinement radii of 20 nm for PbS and 46 nm for PbSe,[4, 30] the absorption and emission peaks of PbQ (Q=S, Se) QDs can be tuned to the near-infrared region (0.4 eV to 1.4 eV). However, the particle size is smaller than 3 nm when their band gap reaches 1.5 eV, which is difficult to synthesize and stabilize.[18] This hinders our ability to tune the absorption and emission peaks of these materials into the visible light.

To alter the electronic structure and optical properties of PbQ (Q=S, Se), an effective way is to change the atomic coordination or crystal structure building motif, which can lead to new structures or new material systems. Introduction of new building motifs with large *HOMO-LUMO* gap into a crystal structure is a logical step.[31-35] Because these building motifs effectively "dilute" the original motif, they can incorporate their own properties into the original crystal matrix and in turn increase the band gap in the synthesized structure.[34-35] In addition, this "dilution" effect may also incorporate states of the new building motif with high *HOMO-LUMO* gap and produce a much complicated electronic structure. For example, the $[P_2S_6]^{4-}$ motif has a *HOMO-LUMO* gap about 4 eV,[36] which is much larger than that of the host PbS matrix. The incorporating of $[P_2S_6]^{4-}$ motif into PbS leads to a new material, namely $Pb_2P_2S_6$. $Pb_2P_2S_6$ crystallizes in the monoclinic space group $P\,2_1/c$.[37] The Pb atoms are coordinated to eight S atoms, forming a distorted square antiprism geometry. Because of the "dilution" effect, $Pb_2P_2S_6$ has a band gap of 2.57 eV,[38] much larger than that of PbS (0.37 eV). In addition, the electronic structure of $Pb_2P_2S_6$ is more complicated than that of PbS. If the excitation of $Pb_2P_2S_6$ is from S-3p/Pb-6s to Pb-6p, as in PbS,[29] there can be another excitation path in $Pb_2P_2S_6$, namely from S-3p to P states. The two excitation paths may result in a multi-band or indirect band material.[35] Previous works had focused mainly on the ferroelectric[36, 39-40] properties. But few of them attempt to tune the band gap energy of the $Pb_2P_2S_6$ material. Furthermore, the size-dependence nature of $Pb_2P_2S_6$ nanoparticles has not been reported.

Herein, in this paper, we focus our attention on the size-dependent properties of the band gap energy of the $Pb_2P_2S_6$ nanoparticles. The high-speed milling technique was used to produce $Pb_2P_2S_6$ nanoparticles. The size dependence of the band gap energy and the corresponding band-edge emission properties were measured. Finally, First-principle calculation was performed in order to understand the electronic structure and semiconducting properties of $Pb_2P_2S_6$.

Results and discussion

Synthesis and morphology

The traditional molten salt method can provide a homogeneous liquid medium at relatively low temperature which is beneficial to the synthesis of well-crystallized and well-defined micro- or

nano-crystalline materials.[46] The LiBr/KBr system with the mole ratio of 3/2 (LiBr/KBr) has a low melting point around 600 K, making it a good reacting medium. **Figure 1a-c** show the SEM image of the $Pb_2P_2S_6$ powders which are obtained under different conditions. Obviously, the $Pb_2P_2S_6$ powder shows high crytallinity, which can be proved further by the XRD results. In molten KI, $Pb_2P_2S_6$ prefers to crystallize in parallel hexahedra shape. The shape changes to truncated parallel hexahedra when molten LiBr/KBr was used as the reacting medium. Decreasing of the concentration of starting materials from 1.5 mmol/g to 0.5 mmol/g does not lead to changes in shape or size (**Figure 1b&c**). The size of the $Pb_2P_2S_6$ particles could be estimated from the SEM image, even though the particles have distinct shape. Note that in the parallel hexahedra case, only the longer edge was measured. The size ranges from 0.5 μm to 5 μm with an average value of 2 μm for the $Pb_2P_2S_6$ particles synthesized in KI flux, while the average size of the $Pb_2P_2S_6$ particles synthesized in the LiBr/KBr flux is 1.3 μm.

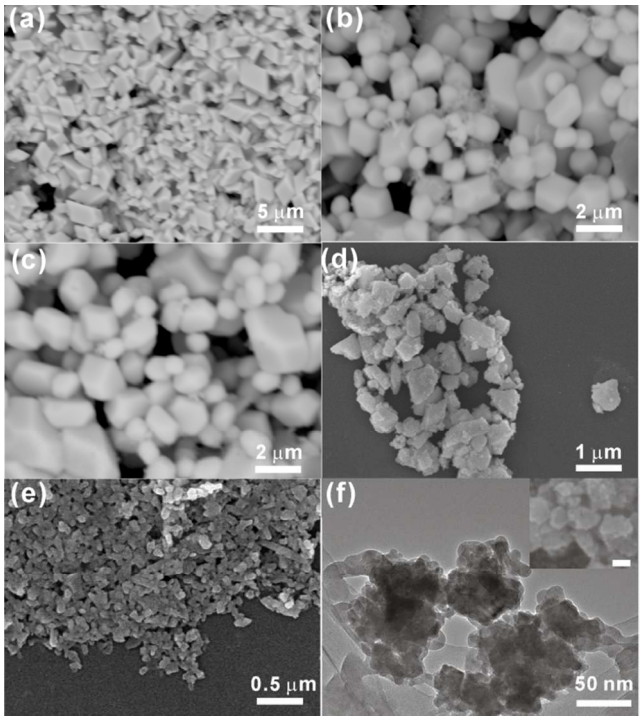

Figure 1. SEM images of $Pb_2P_2S_6$ powder synthesized under different conditions. (a) KI flux, starting materials concentration: 1.5 mmol/g, temperature: 973 K; (b) LiBr/KBr flux, starting materials concentration: 1.5 mmol/g, temperature: 773 K; (c) LiBr/KBr flux, starting materials concentration: 0.5 mmol/g, temperature: 773 K; and milling for 0.5 h (d) and 2 h (e). (f) TEM images of $Pb_2P_2S_6$ powder which was milled for 4 h. Insert is the SEM images of $Pb_2P_2S_6$ powder which was milled for 4 h.

Although in theory changing the reacting condition can lead to different size of the $Pb_2P_2S_6$ particles, further reduction of the size of $Pb_2P_2S_6$ particles could not be achieved in our case. To further reduce the particle size, a high-speed planetary ball milling technique was applied. The morphology of the milled powders with different milling time is illustrated in **Figure 1d-f**. Evidently, the particle size decrease with the increase of milling time. When milled for 0.5 h, the particles have an average size about 0.5 μm, with some size up to 1 μm. When the milling time was increased to 2 h, the size of the $Pb_2P_2S_6$ particles dropped significantly. The average size of the particles is 110 nm, with the largest size up to 200 nm. However, the shape of the particles became irregular, because the planetary ball milling procedure is just a mechanical pulverization process. The nature of this process makes it difficult to control the shape of the particles. When the milling time is up to 4 h, the average size of the particles is 60 nm, which can be obtained by the SEM result (Insert of **Figure 1f**)

Powder X-ray Diffraction and Optical properties

The phase purity of the given powder was checked by PXRD. As illustrated in **Figure 2**, the pattern of the powder sample are indexed (**Figure 2a**) and matched well with the simulated one from $Pb_2P_2S_6$ single crystal data using the *PowderCell* program (**Figure 2b**). No extra peaks were observed. The XRD patterns of the nanostructured $Pb_2P_2S_6$ could all be indexed. The pattern of the unmilled pure sample is also shown for comparison in **Figure 2b**. After milling for different time, the pattern of the nanostructured $Pb_2P_2S_6$ powder become much broader than that of the parental material. This implies the mechanical breaking-up occurred during the high-speed planetary ball milling treatment. Besides, the peak width increases with the milling time. The *Scherrer* equation was used to estimate the grain size of the nanostructured $Pb_2P_2S_6$ powders.[47-48] The three peaks around 16.2°, 17.9° and 18.9°, which correspond to the $(\bar{1}01)$, (011) and (200) planes respectively, are chosen to calculate the grain size. The results are depicted in **Table 1**. With the increase of milling time from 0.5 h to 4 h, the grain size decreases from 52 nm to 8 nm. Due to the aggregation of particles during the milling process, the grain size is much smaller than the particles size. Note that the *Scherrer* equation is applicable for materials with grain size larger than 100 nm, thus the parent $Pb_2P_2S_6$ material is not include in this calculation.

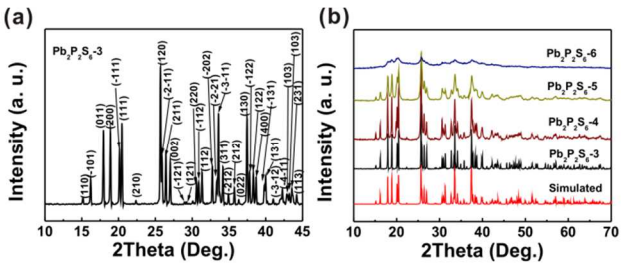

Figure 2. Powder X-ray diffraction patterns of the as-prepared $Pb_2P_2S_6$ powder.

The optical properties of the as-prepared powders were investigated by UV-vis diffuse reflectance spectrum, as depicted in **Figure 3a**. A blue shift of the absorption edge appears when the material is milled. In addition, both the parent and milled samples show absorption tails in the UV-vis spectrum. These absorption tails suggest that the $Pb_2P_2S_6$ compound have an indirect absorption process under illumination. The band gap of the as-prepared powder was estimated from the absorption spectrum by using an extrapolation method, as illustrated in **Figure 3b**. The obtained band gap energy is shown in **Table 1**.

The intrinsic band gap of the $Pb_2P_2S_6$ parent material is 2.56 eV, which is consistent with previous reports.[38] The band gap increases with the decrease of the particle size. When the particle size of the nanostructured $Pb_2P_2S_6$ powders is 60 nm (milling for 4 h), the band gap is 2.88 eV, which is 0.32 eV larger than that of the parental $Pb_2P_2S_6$ material. The band gap energy of the well-known PbS quantum dots has a strong size-dependency. Compared to the PbS quantum dots, $Pb_2P_2S_6$ has an intrinsic band gap of 2.56 eV, which is in the visible light region. Therefore the size-dependence of the band gap energy of the $Pb_2P_2S_6$ material can enable us to tune its photoluminescent properties.

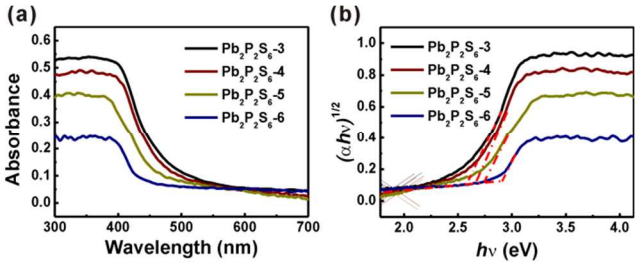

Figure 3. (a) Solid-state UV-vis diffuse reflection spectra of the $Pb_2P_2S_6$ powder with different particle size. (b) The plot of $(\alpha h\nu)^{1/2}$ against photon energy for estimation of directly allowed optical gap using the Kubelka-Munk equation.

Table 1. Summary of the measurement results of $Pb_2P_2S_6$ and nanostructured $Pb_2P_2S_6$ powders.

Sample	Milling time (h)	Grain size (nm) (from XRD)	Average particle size (nm) (from SEM)	Band gap energy (eV)
$Pb_2P_2S_6$-0	0	-	2000	2.56
$Pb_2P_2S_6$-1	0.5	52	500	2.64
$Pb_2P_2S_6$-2	2	33	110	2.72
$Pb_2P_2S_6$-3	4	8	60	2.88

Photoluminescent properties.

The photoluminescence properties of $Pb_2P_2S_6$ and nanostructured $Pb_2P_2S_6$ materials were measured and the typical excitation and emission spectra are depicted in **Figure 4**. By monitoring the emission line at 450 nm, the excitation lines around 400 nm are observed (**Figure 4a**) for $Pb_2P_2S_6$ and nanostructured $Pb_2P_2S_6$ materials. Under the excitation of 400 nm, four strong emission peaks, centered at 468 nm, 473 nm, 482 nm and 493 nm, respectively, appear for the parent $Pb_2P_2S_6$ material (**Figure 4b**). The emission covers the range of blue and green light. This implies that the parental $Pb_2P_2S_6$ and nanostructured $Pb_2P_2S_6$ materials feature multi-band emissions. This character demonstrates that the powder is a possible candidate for mixed color luminescent applications. The peak around 493 nm (2.52 eV) is attributed to the band edge emission of the parental $Pb_2P_2S_6$ material.

After milling, a significant blue shift appears for all nanostructured $Pb_2P_2S_6$ powder, which is consistent with the UV-vis results. The strong emission peaks around 452 nm (2.75 eV) turn out to be the band edge of the parental powder, for their band gap is enlarged with the decrease of the particle size. In addition, a shoulder peak around 440 nm (2.83 eV) stands out, and become significant in the case of the material with small particle size. Compare to the PbS quantum dots, nanostructured $Pb_2P_2S_6$ powder show an tunable emission property in the green-to-blue light region.

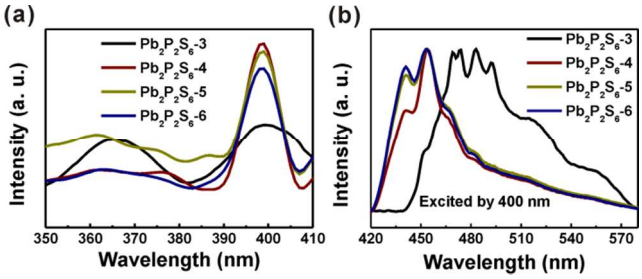

Figure 4. (a) Excitation spectrum of the $Pb_2P_2S_6$ parent and nanostructured $Pb_2P_2S_6$ materials. (b) Emission spectra of the $Pb_2P_2S_6$ parent and nanostructured $Pb_2P_2S_6$ materials excited by 400 nm.

Electronic band structure.

To understand the optical and photoluminescent properties of the $Pb_2P_2S_6$ powder, first-principle calculations were conducted. The electronic band structure of $Pb_2P_2S_6$ is shown in **Figure 5a**. Obviously, the valence band maximum (VBM) is located at *Y* (0.5, 0, 0), while the conduction band minimum (CBM) is at Γ(0, 0, 0). This indicates $Pb_2P_2S_6$ has an indirect band gap. As mentioned previously, the $Pb_2P_2S_6$ powder has a small tail in its UV-vis spectra. The tail is due to the absorption of electrons excited from the VBM to CBM with the energy of 2.15 eV. However, the direct band gap appears at *Y* (0,0,0) with band gap energy of 2.52 eV. The computational results fit well with the UV-vis and photoluminscent measurements.

The total and partial density of states (DOS) are shown in Figure 5b-d. The valence band (VB) mainly consists of S-3*p* and Pb-6*s* orbitals and the conduction band (CB) is mainly the mixture of Pb- and S-orbitals. Even though the P-orbitals contribute less to the CB than Pb- and S-obitals, the main transition of $Pb_2P_2S_6$ with the energy of 2.56 eV contains the contribution of P-obitals. However, the P states have hardly any contribution to the CBM, from which we can conclude that the absorption tail of $Pb_2P_2S_6$ in the UV-vis spectra is from the transition of S-3*p*/Pb-6*s* to Pb-6p. In addition, the CB is not localized but highly diffused. This might be the reason for the broad emission range properties of the $Pb_2P_2S_6$ powder.

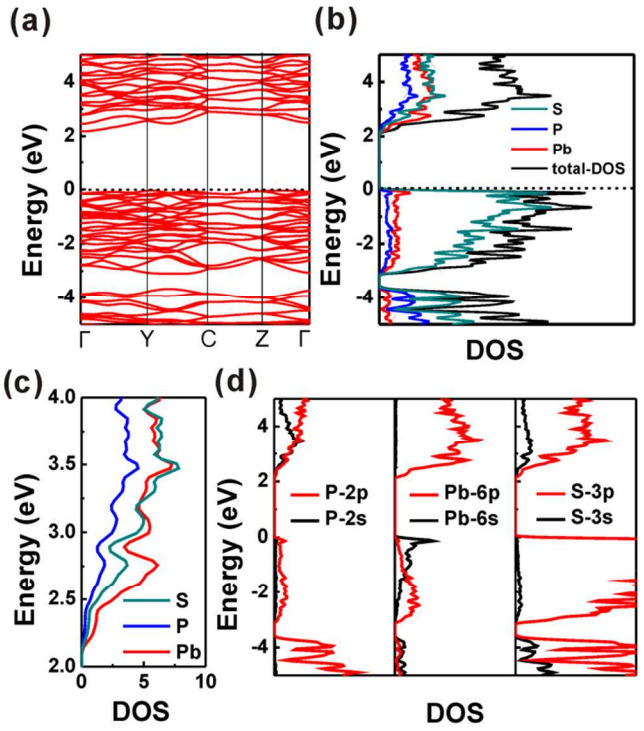

Figure 5. (a) Electronic band structure of $Pb_2P_2S_6$. (b) Total density of states of $Pb_2P_2S_6$. (c) Total density of states of each component in $Pb_2P_2S_6$. (d) Partial density of states of each component in $Pb_2P_2S_6$.

Conclusions

The microcrystalline and nanostructured $Pb_2P_2S_6$ powders were synthesized via a traditional melting salt method with KI or LiBr/KBr mixture (mole ratio 3/2) acting as flux and high-speed planetary ball milling technique, respectively. In KI molten media, we produced highly crystallized $Pb_2P_2S_6$ powder with parallel hexahedra shape and average size around 2 μm. While in LiBr-KBr melting media, $Pb_2P_2S_6$ powder features truncated parallel hexahedra and 1.3 μm in average size. The average size of the nanostructured $Pb_2P_2S_6$ powder decreases from 500 to 60 nm with increasing milling time. The properties of $Pb_2P_2S_6$ show a strong size-dependence. The band gap increases by 0.32 eV when the milling time is 4 h. The size-dependence nature also makes photoluminescence properties tunable. The size decrease leads to a blue shift from 493 nm to 452 nm, and then to 440 nm. First-principle calculations fit well with the experimental results, revealing that the $Pb_2P_2S_6$ is an indirect band material. The VBM consists of S-3p and Pb-6s orbitals, while the CBM is composed of Pb- and S-orbitals. The P orbitals have contribution to the main transition of $Pb_2P_2S_6$ with the energy of 2.56 eV.

Experimental

Synthesis of $Pb_2P_2S_6$

All operations were carried out in an Ar-protected glove box. $Pb_2P_2S_6$ powder was prepared by the traditional melting salt method. A mixture of starting materials of lead powder (3.0 mmol), red phosphorus (3.0 mmol) and sulfur powder (9.0 mmol) was grounded together with a fixed amount of KI or LiBr/KBr (the mole ratio is 3:2) flux. The mixture was loaded into a carbon-coated fused silica tube. The tube was flame-sealed under vacuum (10^{-3} mbar) and heated slowly to 1073 K (with KI acting as flux) or 773 K (with LiBr/KBr acting as flux) with a programmable furnace. After keeping at this temperature for 10 hours, the furnace was turned off. The direct combination reaction at the presence of excess LiBr/KBr flux gave solidified melts. The melts were washed and sonicated by distilled water and dried with acetone. Afterwards the yellow $Pb_2P_2S_6$ powder was obtained. The preparation conditions are summarised in **Table 2**.

Table 2. Sample preparation conditions summary.

Samples	Pb (mmol)	P (mmol)	S (mmol)	Flux (mmol)	Temp. (K)
$Pb_2P_2S_6$-1	3.0	3.0	9.0	KI (30)	1073
$Pb_2P_2S_6$-2	3.0	3.0	9.0	LiBr/KBr (30)	773
$Pb_2P_2S_6$-3	3.0	3.0	9.0	LiBr/KBr (60)	773

Synthesis of $Pb_2P_2S_6$ nanoparticles

The as-prepared $Pb_2P_2S_6$-3 powder was used as starting material to prepare $Pb_2P_2S_6$ nanoparticles by a high-speed planetary ball milling technique. The ball-to-powder weight ratio was about 12:1 and the rotation speed was 1500 rpm. To avoid excessive heating during milling, each 30 min of milling was followed by a 15 min pause. In this way, the nanostructured $Pb_2P_2S_6$ materials with different milling time (0.5 h, 2 h and 4 h) were obtained. The corresponding samples are named by $Pb_2P_2S_6$-4, $Pb_2P_2S_6$-5 and $Pb_2P_2S_6$-6.

Scanning electron microscopy (SEM)

The morphology of the materials was studied by scanning electron microscopy. The as-prepared $Pb_2P_2S_6$ and nanostructured $Pb_2P_2S_6$ materials were sonicated and dispersed in alcohol. Afterwards, a droplet of the suspension was coated onto a fresh silicon slice. The morphology of the materials was examined on a Hitachi S-4800 scanning electron microscope. Elemental compositions were obtained using an *in situ* semi-quantitative energy dispersive X-ray analysis (EDS) unit attached to the SEM. The EDS data were acquired at 15 kV in secondary electron mode.

Powder X-ray Diffraction (PXRD)

The synthesized powder was used to verify the phase purity on a Rigaku X-ray diffractometer (Cu K_α). Simulated patterns were generated using the CrystalMaker program and the CIF of the $Pb_2P_2S_6$ structure[41].

Solid-State UV-vis Spectroscopy

Optical diffuse-reflectance measurements were carried out using a UV-4100 spectrophotometer operating from 800 nm to 300 nm at room temperature. The $BaSO_4$ powder was used as a 100 % reflectance background. The powder sample was spread on a

compacted base of $BaSO_4$ powder. The generated reflectance-versus-wavelength data were used to measure the band gap of the material. The reflectance data were converted to absorbance data using the Kubelka-Munk equation.[42]

Photoluminescent measurements

A fixed amount of the as-prepared $Pb_2P_2S_6$ and nanostructured $Pb_2P_2S_6$ materials were dispersed in alcohol by ultrasound. A Hitachi F-7000 fluorescence spectrophstometer was used to establish the photoluminescent properties of the materials. The operation ranges from 250 nm to 580 nm at room temperature.

Electronic Band Structure Calculations

The first-principles computations based on the density-functional theory (DFT) were performed using the WIEN2K program package.[43] The Perdew-Burke-Ernzerhof (PBE)[44] version of the generalized gradient approximation (GGA) is used to describe the exchange correlation functional and the linearized augmented plane wave (LAPW) method (PAW)[45] method has been used in the present work. The atomic electron configuration for Pb treats 6*s, 6p* states as valence states, and the others are described by 3*s*, 3*p* valence states for P and S, respectively. The muffin tin radii (R_{MT}) of 2.23, 1.97, 1.74 bohr for Pb, P, and S were used for $Pb_2P_2S_6$. Here, the cutoff energy of plane wave was chosen at 350 eV. For the structure optimizations, 6×6×6 Monkhorst-Pack grids were used for the primitive cell and 4×4×4 k-points for the conventional cell, respectively. The relaxation of geometry optimization was performed until the total energy changes within 10^{-6} eV/atom and the Hellmann-Feynman force on all atomic sites was less than 0.01 eV /Å.

Notes and references

* Corresponding authors.
[a] *College of Chemistry and Molecular Engineering, Peking University, Beijing 100871, China. E-mail: huangfq@pku.edu.cn*
[b] *Shanghai Institute of Ceramics, Chinese Academy of Sciences, Shanghai 200050, China. E-mail: huangfq@mail.sic.ac.cn*
[c] *College of Engineering, Peking University, Beijing 100871, China*
[d] *Department of Chemistry and Biochemistry, Northern Illinois University, DeKalb, IL 60115, USA*
[e] *Department of Chemistry, College of Sciences, Northeastern University, Shenyang 110819, China*

1. L. E. Brus, *J. Chem. Phys.*, 1984, **80**, 4403-4409.
2. A. I. Ekimov, A. L. Efros and A. A. Onushchenko, *Solid State Commun.*, 1985, **56**, 921-924.
3. A. P. Alivisatos, *Science*, 1996, **271**, 933-937.
4. F. W. Wise, *Acc. Chem.Res.*, 2000, **33**, 773-780.
5. C. B. Murray, D. J. Norris and M. G. Bawendi, *J. Am. Chem. Soc.*, 1993, **115**, 8706-8715.
6. R. Plass, S. Pelet, J. Krueger, M. Gratzel and U. Bach, *J. Phys. Chem. B*, 2002, **106**, 7578-7580.
7. R. J. Ellingson, M. C. Beard, J. C. Johnson, P. R. Yu, O. I. Micic, A. J. Nozik, A. Shabaev and A. L. Efros, *Nano Lett.* 2005, **5**, 865-871.
8. S. A. McDonald, G. Konstantatos, S. G. Zhang, P. W. Cyr, E. J. D. Klem, L. Levina and E. H. Sargent, *Nat. Mater.,* 2005, **4**, 138-U114.
9. H. W. Hillhouse and M. C. Beard, *Curr. Opin. Colloid In.*, 2009, **14**, 245-259.
10. H. Lee, H. C. Leventis, S. J. Moon, P. Chen, S. Ito, S. A. Haque, T. Torres, F. Nuesch, T. Geiger, S. M. Zakeeruddin, M. Gratzel and M. K. Nazeeruddin, *Adv. Funct. Mater.,* 2009, **19**, 2735-2742.
11. W. Ma, J. M. Luther, H. M. Zheng, Y. Wu and A. P. Alivisatos, *Nano Lett.,* 2009, **9**, 1699-1703.
12. H. Bi, F. Huang, J. Liang, Y. Tang, X. Lü, X. Xie and M. Jiang, *J. Mater. Chem.*, 2011, **21**, 17366-17370.
13. J. Tang, K. W. Kemp, S. Hoogland, K. S. Jeong, H. Liu, L. Levina, M. Furukawa, X. H. Wang, R. Debnath, D. K. Cha, K. W. Chou, A. Fischer, A. Amassian, J. B. Asbury and E. H. Sargent, *Nat. Mater.*, 2011, **10**, 765-771.
14. J. Tang, H. Liu, D. Zhitomirsky, S. Hoogland, X. Wang, M. Furukawa, L. Levina and E. H. Sargent, *Nano Lett.*, 2012, **12**, 4889-4894.
15. Y. Yang, L. Zhu, H. Sun, X. Huang, Y. Luo, D. Li and Q. Meng, *ACS Appl. Mater. Inter.*, 2012, **4**, 6162-6168.
16. L.-Y. Chang, R. R. Lunt, P. R. Brown, V. Bulović and M. G. Bawendi, *Nano Lett.*, 2013, **13**, 994-999.
17. G.-H. Kim, H.-B. Kim, B. Walker, H. Choi, C. Yang, J. Park and J. Y. Kim, *ACS Appl. Mater. Inter.*, 2013, **5**, 1757-1760.
18. W. Yoon, J. E. Boercker, M. P. Lumb, D. Placencia, E. E. Foos and J. G. Tischler, *Sci. Rep.*, 2013, **3**.
19. H. Fu and S.-W. Tsang, *Nanoscale*, 2012, **4**, 2187.
20. I. Moreels, Y. Justo, B. De Geyter, K. Haustraete, J. C. Martins and Z. Hens, *Acs Nano*, 2011, **5**, 2004-2012.
21. I. Moreels, K. Lambert, D. Smeets, D. De Muynck, T. Nollet, J. C. Martins, F. Vanhaecke, A. Vantomme, C. Delerue, G. Allan and Z. Hens, *Acs Nano*, 2009, **3**, 3023-3030.
22. F. W. W. Inuk Kang, *J. Opt. Soc. Am. B*, 1997, **14**, 1632-1646.
23. A. Olkhovets, R. C. Hsu, A. Lipovskii and F. W. Wise, *Phys. Rev. Lett.*, 1998, **81**, 3539-3542.
24. M. A. Hines and G. D. Scholes, *Adv. Mater.*, 2003, **15**, 1844-1849.
25. J. M. Pietryga, R. D. Schaller, D. Werder, M. H. Stewart, V. I. Klimov and J. A. Hollingsworth, *J. Am. Chem. Soc.*, 2004, **126**, 11752-11753.
26. L. Cademartiri, E. Montanari, G. Calestani, A. Migliori, A. Guagliardi and G. A. Ozin, *J. Am. Chem. Soc.*, 2006, **128**, 10337-10346.
27. J. E. Murphy, M. C. Beard, A. G. Norman, S. P. Ahrenkiel, J. C. Johnson, P. R. Yu, O. I. Micic, R. J. Ellingson and A. J. Nozik, *J. Am. Chem. Soc.*, 2006, **128**, 3241-3247.
28. T.-Y. Liu, M. Li, J. Ouyang, M. B. Zaman, R. Wang, X. Wu, C.-S. Yeh, Q. Lin, B. Yang and K. Yu, *J. Phys. Chem. C*, 2009, **113**, 2301-2308.
29. S. E. Kohn, P. Y. Yu, Y. Petroff, Y. R. Shen, Y. Tsang and M. L. Cohen, *Phys. Rev. B*, 1973, **8**, 1477-1488.
30. A. L. Rogach, A. Eychmüller, S. G. Hickey and S. V. Kershaw, *Small*, 2007, **3**, 536-557.
31. F. Q. Huang, P. Brazis, C. R. Kannewurf and J. A. Ibers, *J. Solid State Chem.*, 2000, **155**, 366-371.
32. F. Q. Huang and J. A. Ibers, *Inorg. Chem.*, 2001, **40**, 2602-2607.
33. M.-L. Liu, L.-B. Wu, F.-Q. Huang, L.-D. Chen and I. Chen, *J. Appl. Phys.*, 2007, **102**, 116108-116108-116103.
34. X. Zhang, W. Chen, D. Mei, C. Zheng, F. Liao, Y. Li, J. Lin and F. Huang, *J. Alloy Compd.*, 2014, http://dx.doi.org/10.1016/j.jallcom.2014.1005.1086.
35. X. Zhang, J. He, W. Chen, K. Zhang, C. Zheng, J. Sun, F. Liao, J. Lin and F. Huang *Chem. –Eur. J.*, 2014, **20**, 5977-5982.
36. K. Glukhov, K. Fedyo, J. Banys and Y. Vysochanskii, *I Int. J. Mol. Sci.*, 2012, **13**, 14356-14384.
37. W. Klingen, R. Ott and H. Hahn, *Z. Anorg. Allg. Chem.*, 1973, **396**, 271-278.
38. C. Calareso, *Appl. Phys. Lett.,* 2000, **513**, 59-62.
39. P. P. Guranich, E. I. Gerzanich, A. G. Slivka, V. S. Shusta and V. A. Bobela, *Ferroelectrics*, 1992, **132**, 173-183.
40. V. S. Shusta, E. I. Gerzanich, A. G. Slivka, P. P. Guranich and V. A. Bobela, *Ferroelectrics*, 1993, **145**, 61-71.
41. C. D. Carpentier and R. Nitsche, *Mater. Res. Bull.*, 1974, **9**, 401-410.
42. G. Kortüm, W. Braun and G. Herzog, *Angew. Chem. Inter. Ed. Engl.*, 1963, **2**, 333-341.
43. P. Blaha, K. Schwarz, G. K. H. Madsen, D. Kvasnicka and J. Luitz, {K}arlheinz Schwarz, Techn. Universität Wien, Austria, Wien, Austria, 2001.
44. J. P. Perdew, K. Burke and M. Ernzerhof, *Phys. Rev. Lett.*, 1996, **77**, 3865-3868.
45. P. E. Blöchl, *Phys. Rev. B*, 1994, **50**, 17953-17979.

46. X. Liu, N. Fechler and M. Antonietti, *Chem. Soc. Rev.*, 2013, **42**, 8237-8265.
47. P. Scherrer, *Nachrichten von der Gesellschaft der Wissenschaften zu Göttingen, Mathematisch-Physikalische Klasse*, 1918, **1918**, 98-100.
48. A. L. Patterson, *Phys. Rev.*, 1939, **56**, 978-982.